AGU ADVANCING EARTH AND SPACE SCIENCES

Geophysical Research Letters®

RESEARCH LETTER
10.1029/2023GL105317

Sub-Hourly Observations of Dust Storm Growth, Lee Waves, and Lyot Crater, by the EMM Camera EXI

C. Gebhardt[1,2], B. K. Guha[2], R. M. B. Young[1,2], M. J. Wolff[3], and C. S. Edwards[4]

[1]Department of Physics, College of Science, United Arab Emirates University, Al Ain, United Arab Emirates, [2]National Space Science and Technology Center, United Arab Emirates University, Al Ain, United Arab Emirates, [3]Space Science Institute, Boulder, CO, USA, [4]Department of Astronomy and Planetary Science, Northern Arizona University, Flagstaff, AZ, USA

Key Points:

- The Emirates Mars Mission provided thirteen (sub-)hourly images; they show variations in clouds and atmospheric dust on 18 December 2022
- The image sequence tracks the evolution of both lee waves and a local dust storm between sunrise and mid-afternoon, near Lyot Crater
- We relate our observations to atmospheric dynamics, supported by the Mars Climate Database and radio occultation measurements

Supporting Information:

Supporting Information may be found in the online version of this article.

Correspondence to:

C. Gebhardt,
claus.gebhardt@uaeu.ac.ae

Citation:

Gebhardt, C., Guha, B. K., Young, R. M. B., Wolff, M. J., & Edwards, C. S. (2023). Sub-hourly observations of dust storm growth, lee waves, and Lyot Crater, by the EMM camera EXI. *Geophysical Research Letters*, *50*, e2023GL105317. https://doi.org/10.1029/2023GL105317

Received 4 JUL 2023
Accepted 27 NOV 2023

Author Contributions:

Conceptualization: C. Gebhardt
Data curation: M. J. Wolff, C. S. Edwards
Formal analysis: C. Gebhardt, B. K. Guha
Funding acquisition: C. Gebhardt, R. M. B. Young
Investigation: C. Gebhardt, B. K. Guha
Methodology: C. Gebhardt, B. K. Guha
Project Administration: C. Gebhardt, R. M. B. Young
Resources: M. J. Wolff
Software: C. Gebhardt, B. K. Guha
Visualization: C. Gebhardt, B. K. Guha
Writing – original draft: C. Gebhardt

Abstract We explore a sequence of 13 unique high-cadence images of a dust storm, from the Emirates Mars Mission (EMM). The Emirates eXploration Imager camera took these images in less than 8 hr on 18 December 2022 (Martian Year 36, solar longitude 356°). Most of these images are separated by a time difference of half an hour. The region of interest extends from Lyot crater to the east. During the morning, the EMM images show lee waves (atmospheric gravity waves). In the late morning, the lee waves rapidly change into clearly distinct dust storm texture/convective features. We track the evolution of both lee waves and a local dust storm between sunrise and mid-afternoon. Also, we relate our observations to atmospheric dynamics. Our analysis is supported by the Mars Climate Database and radio occultation measurement data.

Plain Language Summary The Emirates Mars Mission (EMM) has an on-board camera, whose images from 18 December 2022 show a dust storm near Lyot crater (a large crater in the northern hemisphere of Mars). An image was taken almost every half an hour. In total, this gave 13 camera images in less than 8 hr. This number of images in such a short time is unique. The images reveal clouds which form straight lines during the morning. Such straight clouds are known as "lee wave clouds." In the late morning, the lee waves disappear quickly and a quite different dust cloud appears. The latter is a dust storm which grows quickly. We follow the lee waves and dust storm from sunrise to mid-afternoon. Also, we put our observations into the context of physical processes in the Mars atmosphere. Our work is supported by external data and measurements. That is to say data from the Mars Climate Database and radio occultation measurements.

1. Introduction

1.1. Lee Wave Clouds on Mars

Lee waves are atmospheric gravity waves. They form when the atmosphere is stable and wind flows over a topographic obstacle (Kahn, 1984; Pickersgill & Hunt, 1982; Wang & Ingersoll, 2002; and references therein). This includes obstacles, such as mountains (Ogohara & Ro, 2023) and craters (Pickersgill & Hunt, 1979; Wood et al., 2003). The vertical displacement of air initiates a vertical oscillation with atmospheric buoyancy acting as a restoring force. This results in a pattern of alternating upward and downward winds on the lee side of the obstacle, that means a lee wave. Adiabatic cooling can generate water-ice clouds where the motion is upward. Such lee wave clouds can form straight lines, perpendicular to the mean wind direction. In addition, they can form a ship-wake pattern. Lee wave clouds have a seasonality. They are absent around summer solstice in the northern hemisphere of Mars. Their activity tends to increase from late northern summer to fall (Wang & Ingersoll, 2002; Wood et al., 2003). Lee wave clouds occur around craters with sizes from few to hundreds of kilometers. For large craters, lee wave clouds may extend up to 1,000 km in the down-wind direction.

Lee wave clouds are characterized by the Scorer parameter l and buoyancy frequency N, which depend on the potential temperature θ, horizontal wind speed U, altitude z, and Mars gravity g (Ogohara & Ro, 2023; Wood et al., 2003; and references therein). The buoyancy frequency is given by

$$N = \sqrt{\frac{g}{\theta}\frac{d\theta}{dz}}, \tag{1}$$

the Scorer parameter by

Writing – review & editing: B. K. Guha, R. M. B. Young, M. J. Wolff

$$l = \sqrt{\frac{N^2}{U^2} - \frac{\frac{d^2U}{dz^2}}{U}}, \quad (2)$$

and Mars gravity by

$$g = 3.71\,\mathrm{ms}^{-2}. \quad (3)$$

The Scorer parameter may be considered a wave number and converted into wavelength. This gives the Scorer wavelength. The Scorer wavelength may increase significantly with altitude and thus limit the vertical propagation of lee waves. This results in trapped lee waves. That is because lee waves can only propagate vertically if their wavelength is larger than the Scorer wavelength (or, conversely, if their wavenumber is smaller than the Scorer parameter). In the horizontal direction, trapped lee waves are stationary waves, aligned with the mean wind direction.

1.2. The Region of Interest, Including Lyot Crater

The map in Figure 1a shows the geographical context of this study. The region of interest (ROI) extends eastward from Lyot crater, whose central coordinates are approximately 50.8°N and 29.3°E. To the east, north, and west, the crater is surrounded by low plains. The dichotomy boundary is directly south of Lyot crater, including the region Deuteronilus Mensae. Lyot crater is one of the largest impact craters of the northern plains (Brooker et al., 2018; and references therein). It has a maximum depth of 3 km and includes the lowest point in the northern hemisphere of Mars. The crater has also a central peak, mountain ring, crater rim, and ejecta blanket. The crater diameter is around 215 km. Lyot crater is of scientific interest for various reasons. These include its large size, young age, location in the northern hemisphere, hydrological activity, and aeolian processes (Brooker et al., 2018; Dickson et al., 2009; Harrison et al., 2010; Weiss et al., 2017; and references therein).

The topography of Lyot crater may be an essential factor for generating the observed lee waves, described in Section 3. Also, any generalizable knowledge on the behavior of dust storms adjacent to craters may be directly relevant for observations by surface missions (Lemmon et al., 2022; Ordonez-Etxeberria et al., 2019, 2020).

1.3. The EMM Camera EXI

The Emirates Mars Mission (EMM, AlMatroushi et al., 2021; Amiri et al., 2022) of the United Arab Emirates is the first Mars mission by an Arab country. The EMM science orbit has altitudes between 20,000 (periapsis) and 43,000 km (apoapsis), with an inclination of 25°. The orbital period is 55 hr. EMM officially began science operation on 23 May 2021. This date is equivalent with Martian Year (MY) 36, solar longitude (L_S) 49°. EMM completed one Martian Year of science operation in April 2023.

The EMM instrument Emirates eXploration Imager (EXI, Jones et al., 2021) provides camera images of the Mars atmosphere and surface. The EXI camera has six spectral bands. Three visible bands are centered around wavelengths of 635, 546, and 437 nm. Three ultraviolet bands are centered around wavelengths of 320, 260, and 220 nm. They are also known as f635, f546, f437, f320, f260, and f220, respectively. The spatial image resolution varies between the periapsis and apoapsis of the EMM orbit, between around 2–4 km per pixel in the nadir looking direction. The ground size of a pixel increases by a factor of 1/cosine(emission angle) for off-nadir looking directions.

All EXI images used in this work were downloaded from the EMM Science Data Center (https://sdc.emirates-marsmission.ae/). Figure 2 and Movie S1 are based on level 2B images, which come with a map-projection (Jeppesen et al., 2021). Figure 3 is based on level 2A images, which were used in the same way as in Gebhardt et al. (2022).

This article is structured as follows. Section 2 is an overview of the considered EXI high-cadence image sequence. Section 3 studies the observed lee waves and related aspects of planetary boundary layer dynamics. Section 4 describes how the local dust storm grows on sub-hour time scales. Section 5 are the study conclusions and summary.

2. EXI High-Cadence Images of a Dust Storm

The EXI camera has different observation modes. The routine observation mode XOS1 takes images at a time step of approximately 2.5 hr (Amiri et al., 2022). That is routine cadence. Each XOS1 image is a chain of visible

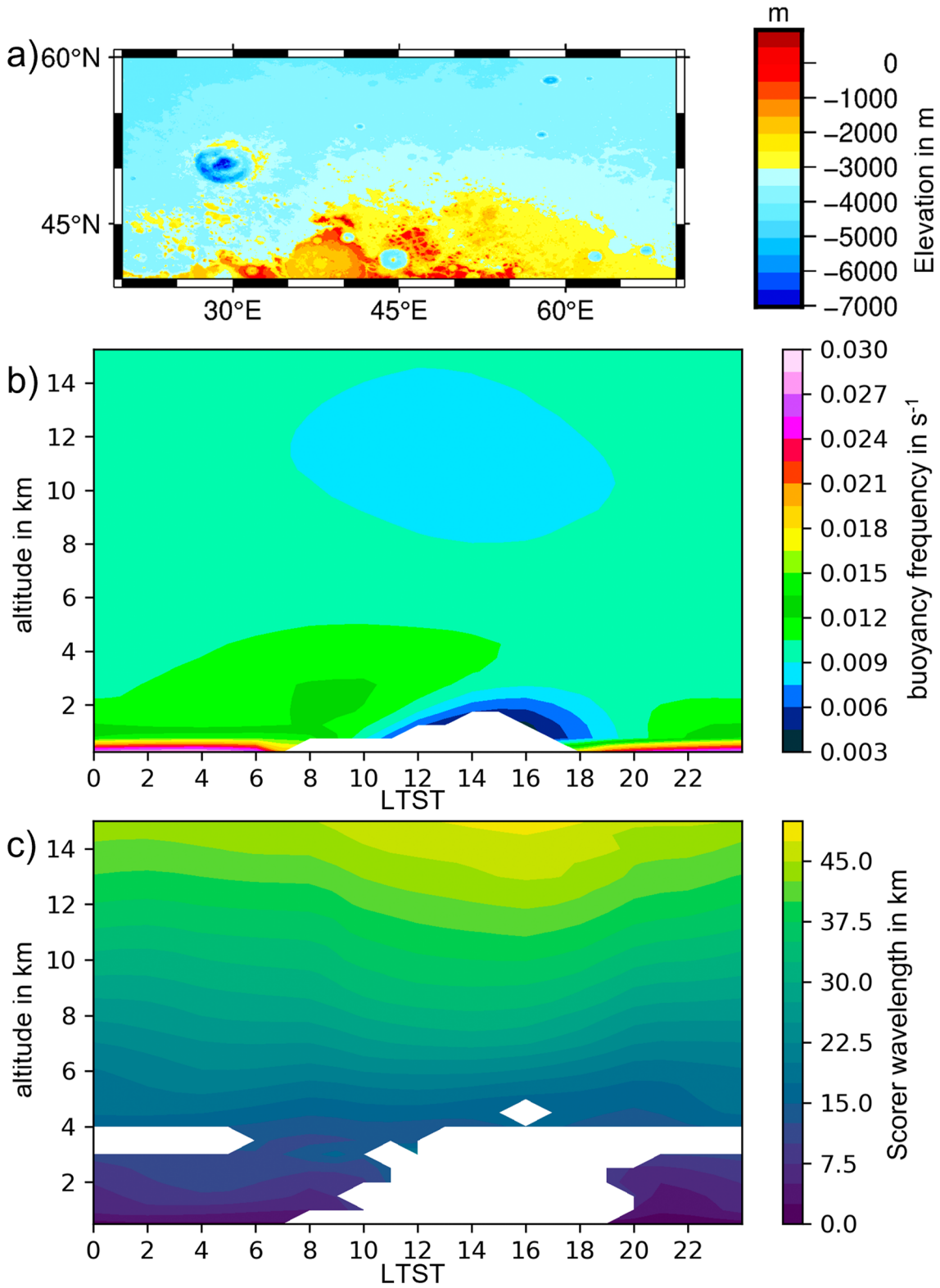

Figure 1.

and ultraviolet sub-images, using different EXI spectral bands. Gebhardt et al. (2022) used a sequence of five XOS1 images on 10 September 2021, with a time step of around 2–3 hr. The specialized observation modes XOS6 and XOS7 take image sequences at a sub-hour time step. That is high-cadence. The basis of this article are high-cadence images of a local dust storm on 18 December 2022. They show rapidly evolving changes of dust storm characteristics over a sub-hour time scale.

EXI provided high-cadence images of the ROI (see Section 1.2) on 18 December 2022. Table 1 lists these 13 images, numbered from image0 to image12. Also, the EXI observation mode (XOS6 and XOS1) and Earth Coordinated Universal Time (UTC) are provided. The time step between images is typically around half an hour, except in two cases, when the time step is around 1 hr. In total, images0-12 were taken in less than 8 hr.

EXI imaged the ROI from sunrise through afternoon, beginning at local true solar time (LTST) 7.1 at longitude 45°E in image0 and ending at LTST 14.7 in image12. After that, the ROI vanished at the horizon. From images0-12 in Table 1, the sub-spacecraft longitude changed from 42.1°E to −38.9°E, the sub-spacecraft latitude from 8.8°N to 19.9°N, and the spacecraft altitude from around 41,500 to 35,200 km.

We selected the images in Table 1 for this study because they show the growth of a local dust storm, together with lee waves observed east of Lyot crater. The dust storm and lee waves are clearly visible in the color images and related 635 nm images from EXI. As an example, Figure 2 shows parts of images6-8 as map-projected color images. The Movie S1 shows the sequence of all such map-projected color images, that is, image0 through image12. In Figure 3, 635 nm images are used for detailed study of the observed dust storm. This approach is consistent with the use of EXI color and 635 nm images in Gebhardt et al. (2022). Note also that EXI 320 nm images cannot be used here as in Gebhardt et al. (2022). That is because the ROI is largely masked by the northern polar hood (NPH), which is very bright in the 320 nm images. The polar hood is known to have altitudes up to 40 km (Benson et al., 2011). By contrast, we study lee waves trapped below approximately 10 km, see Section 3.

3. Lee Wave Clouds

Figures 2 and 3 clearly show that lee waves are visible in the color and 635 nm images. In those images, super-imposed water ice clouds of the NPH do not obfuscate the ROI in the same way as in the 320 nm images. At the considered time of the year, $L_S = 356°$, the NPH is known to extend southward of 60°N (Wang & Ingersoll, 2002). NPH clouds may include cloud hazes as well as streak clouds, which often spiral counterclockwise toward the pole in north polar maps. It is widely known that NPH clouds often co-exist with lee waves. For instance, a close look at Figure 6f of Wang and Ingersoll (2002) shows NPH clouds and lee wave clouds around and to the east of Lyot crater, which is similar to the lee waves studied here. Lee waves are not easily confused with other clouds, such as NPH clouds and atmospheric fronts, because of their unique multi-streak texture (Ogohara & Ro, 2023).

Figure 3 shows that there are lee wave clouds in a broad region around Lyot crater. Some of the most distinct lee wave structure is over the crater and to its east and south. There are long wave trains, where the lee wave clouds form coherent cloud bands. We estimated their wavelength by visual inspection, using a method similar to Ogohara and Ro (2023). We selected a wave train to the south of Lyot crater and drew a line perpendicular to the cloud bands (red arrows in Figures 3b–3d). This enclosed 8, 9, and 11 cloud bands from image1, image2, and image3, respectively. We determined the wavelength by dividing the line length by the cloud band number. This gave a wavelength of around 32 km for image1, 31 km for image2, and 31 km for image3. Each of these estimates includes an uncertainty of up to few kilometers, consistent with the EXI ground pixel size, described in Section 1.3.

To constrain the altitude of the lee waves, we obtained data on the potential temperature and horizontal wind from the Mars Climate Database (MCD, http://www-mars.lmd.jussieu.fr/). We used these data in vertical steps of 0.5 km, over the same latitude and longitude range and solar longitude as our observation of distinct lee waves around Lyot crater. Figures 1b and 1c show the resulting buoyancy frequency and Scorer wavelength, as a

Figure 1. (a) This is a topographic map of the region of interest. Lyot Crater is the dark blue feature in the center-left, around 50°N and 30°E. The map shows the same area as the map-projected Emirates Mars Mission images in Figures 3a–3m. The map is based on Mars Orbiter Laser Altimeter high-resolution topography (32 pixels per degree, available from the Mars Climate Database [MCD]) (b, c) show the buoyancy frequency and Scorer wavelength as a function of the local true solar time and above-surface-height. Both were estimated over latitudes from 44°N to 56°N and longitudes from 30°E to 39°E, in steps of 3°, and then averaged. This was done by using potential temperature and horizontal wind data from the MCD, version 6.1 (http://www-mars.lmd.jussieu.fr/) for solar longitude 356°, in vertical steps of 0.5 km. The blank spaces in panel (b) are data points with negative buoyancy frequency (i.e., an unstable atmosphere, which is not conducive to lee waves) and in panel (c) a negative Scorer parameter.

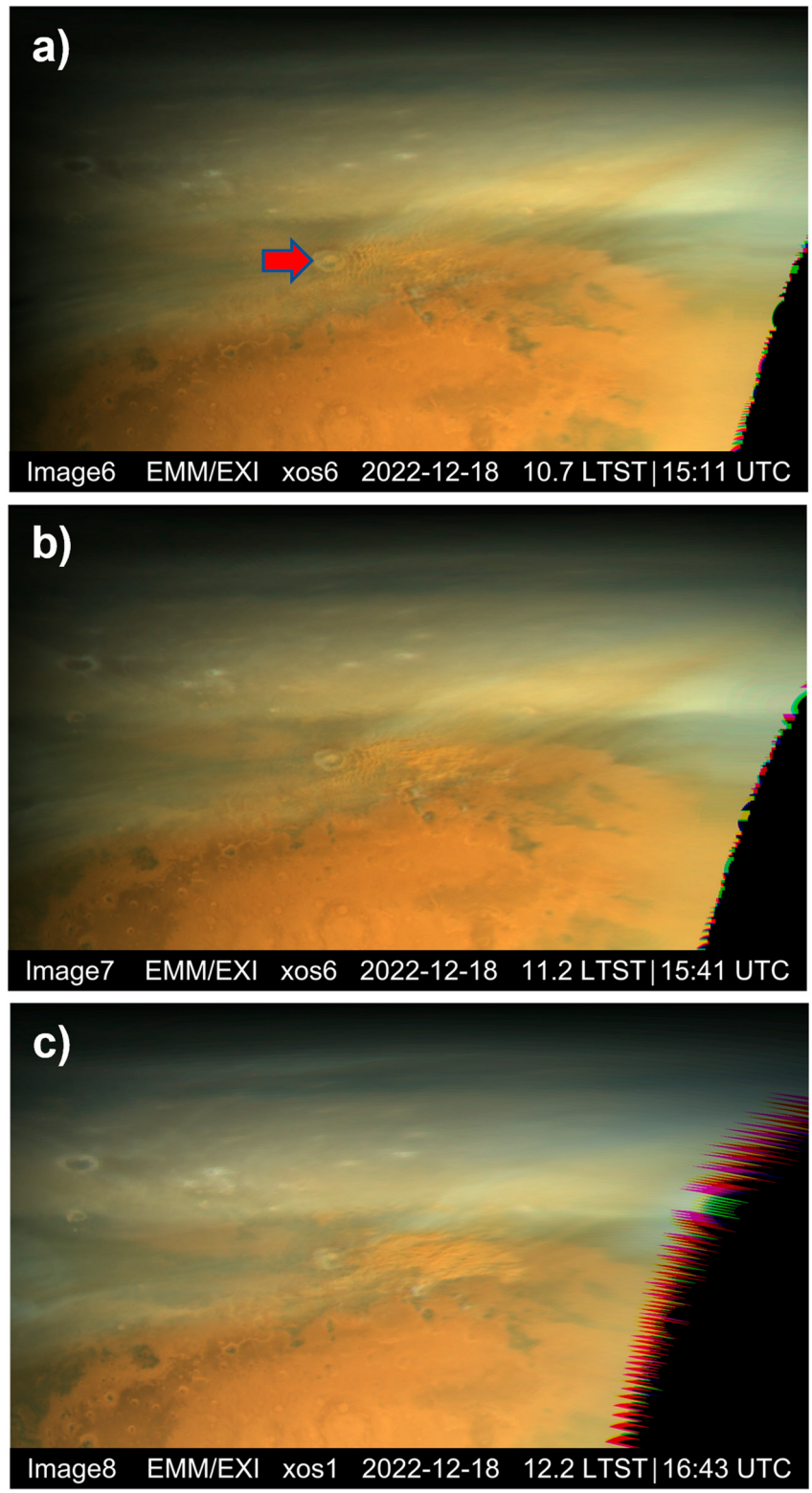

Figure 2. Map-projected Emirates eXploration Imager color images showing the growth of a local dust storm. Panels (a–c) show selected parts of images6–8, listed in Table 1. Lyot crater is slightly left of the middle, highlighted by an arrow in panel (a). In panel (c), the local dust storm is evident east and south of Lyot crater. The northern part of panels (a–c) shows the CO_2-rich polar cap ice. At the considered time of the year, $L_S = 356°$, the CO_2-rich polar cap ice extends to the northern midlatitudes (Appéré et al., 2011).

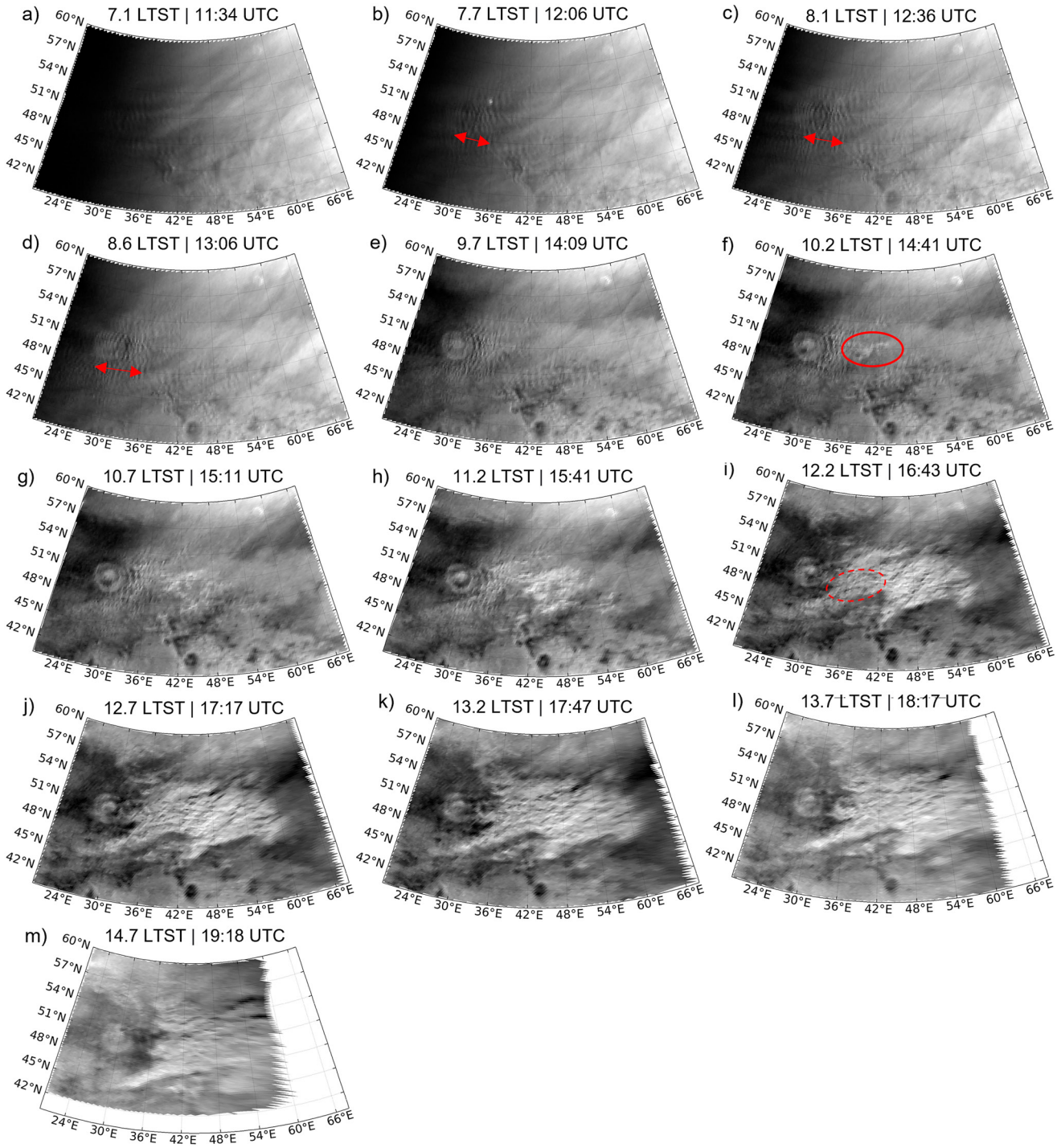

Figure 3. This sequence of Emirates eXploration Imager (EXI) 635 nm images shows lee waves and the development of a local dust storm near Lyot crater. Each panel shows a map projection of some selected part of an EXI image. This starts with image0 in panel (a) and ends with image12 in panel (m). Lyot crater is around 50.8°N and 29.8°E, in the middle-left of each panel. There is a wave pattern in panels (a–h) over, east, and south of Lyot crater. These are lee waves. Wave trains to the south of Lyot crater are highlighted by red arrows in panels (b–d). We used these wave trains to estimate the wavelength of the lee waves. In panels (f–m), there are dust storm texture/convective features, which are clearly distinct from the lee waves. The first observed instance of such dust storm texture/convective features is highlighted by a red circle in image5, see panel (f). The dashed red circle in panel (i) is the approximate area of dust optical depth data by another Emirates Mars Mission instrument, the Emirates Mars Infrared Spectrometer, considered in Section 4.

Table 1
Properties of a Sequence of 13 Images From the Emirates Mars Mission Camera Emirates eXploration Imager (EXI)

Image number	EXI observation mode	Earth UTC on 18 December 2022 (HH:MM:SS)	Mars LTST at 45°E	Sub-spacecraft longitude (°E)	Sub-spacecraft latitude (°N)	Spacecraft altitude (km)
Image0	XOS1	11:34:02	7.1	42.1	8.8	41,531
Image1	XOS6	12:06:24	7.7	36.1	9.6	41,252
Image2	XOS6	12:36:26	8.1	30.6	10.3	40,971
Image3	XOS6	13:06:29	8.6	25.1	11.0	40,670
Image4	XOS1	14:09:09	9.7	13.7	12.6	39,973
Image5	XOS6	14:41:31	10.2	7.9	13.4	39,578
Image6	XOS6	15:11:34	10.7	2.6	14.1	39,189
Image7	XOS6	15:41:37	11.2	−2.7	14.8	38,780
Image8	XOS1	16:43:30	12.2	−13.4	16.3	37,874
Image9	XOS6	17:17:26	12.7	−19.2	17.1	37,342
Image10	XOS6	17:47:28	13.2	−24.2	17.8	36,849
Image11	XOS6	18:17:31	13.7	−29.1	18.5	36,337
Image12	XOS1	19:18:37	14.7	−38.9	19.9	35,238

Note. Most images are separated by around half an hour. Two images are separated by around 1 hr (third column). The Mars local true solar time (LTST) is provided for the longitude of 45°E (fourth column), which is in the middle of the ROI.

function of altitude and LTST. They were calculated using Equations 1 and 2, respectively. Figure 1c shows that the Scorer wavelength increases significantly with altitude. As described in Section 1.1, the condition for vertical propagation of lee waves is that their wavelength must be larger than the Scorer wavelength. From that, we conclude that the considered lee waves of around 30 km wavelength are trapped at altitudes below approximately 10 km. That is consistent with the lee wave cloud climatology produced by Ogohara and Ro (2023) for the east of the Phlegra Montes, which have a similar latitude as Lyot crater.

The lee waves in images1-3 are visible in Figures 3b–3d as cloud bands, and their general direction is oriented from north-to-south. As pointed out in Section 1.1, the cloud bands of trapped lee waves are perpendicular to the mean wind direction. Hence, the lee waves in Figures 3b–3d indicate westerly winds below approximately 10 km. This is consistent with a priori knowledge from the assimilation of observations into models. Around the considered time of year, $L_S = 356°$, zonal winds at northern mid and high latitudes are westerly from the surface to high altitude (e.g., Haberle et al., 2017; their Figure 9.9).

The lee waves clearly change through the morning. The lee waves are obvious at sunrise in Figures 3b–3d, when the atmosphere is stably stratified. All lee waves have disappeared by local noon in Figure 3i. Some lee waves might be obscured by the local dust storm. The fact that not only those, but also other lee waves disappear is consistent with the development of the convective planetary boundary layer (CPBL). The blank spaces in Figure 1b (negative buoyancy frequency) show that the CPBL develops and deepens through the morning. By 14–15 LTST, the CPBL has the maximum height of around 2 km. The latter agrees with radio occultation measurements in Hinson et al., 2019, their Table 2. They found CPBL height of 2–3 km by 14 LTST around the here considered season and latitude ($L_S = 356°$ and around 50°N). The radio occultation measurements of Hinson et al. (2019) have a vertical resolution of 0.5 km. Figures 1b and 1c are based on data from the Mars Climate Database (MCD), which have a vertical step of 0.5 km, accordingly.

Finally, the growth of the local dust storm described in Section 4 is consistent with the presence of the CPBL from mid-morning to late afternoon. If dust is lifted by surface wind stress, the CPBL is essential for the vertical transport of dust (Haberle et al., 2017; Newman et al., 2002).

4. The Growth of a Local Dust Storm Over a Sub-Hour Time Scale

Figures 3f–3h are part of images5–7 and show a rapid transition of structure. There are still lee waves around Lyot crater. But, the lee wave clouds rapidly change into clearly distinct dust storm texture/convective features.

The latter emerge farther east of Lyot crater. We first noticed such dust storm texture in image5, as highlighted by a red circle in Figure 3f. And, the distance between the dust storm texture and the crater rim is around one crater diameter. Figures 3f–3i show that the dust storm texture rapidly expands in the east-to-west direction, which is consistent with the westerly winds, deduced in Section 3 from lee waves.

Figures 3i–3m are part of images8–12. They show the ROI at local times from noon to mid afternoon. Dust storm texture/convective features are dominant east of Lyot crater. Also, they extend southward of Lyot crater. Note that the dust storm texture/convective features do not extend into Lyot crater. They are separated from the eastern and southern crater rim by a distance of roughly half a crater diameter.

A closer look at Figures 3i–3m reveals that the dust storm texture/convective features include structures, that are elongated in the east-to-west direction. This is in line with the westerly winds, deduced from lee waves in Section 3. The dust storm texture/convective features are also consistent with the cellular or granular texture of polar cap edge dust storms in Sánchez-Lavega et al. (2022). These aspects corroborate that the dust storm texture/convective features have a clearly different appearance than the preceding lee waves, described above.

Figures 3i–3m show that the dust storm also expands toward the north. Eventually, dust storm activity is visible to the north-east of Lyot crater, close to the polar cap edge. As expected, the observed dust storm is consistent with a polar cap edge dust storm.

The area, centroid latitude, and centroid longitude of the dust storm are

1. 2.21×10^5 km^2, 49.566°N, 47.287°E in image7, see Figure 3h
2. 6.47×10^5 km^2, 50.144°N, 44.444°E in image8, see Figure 3i
3. 6.74×10^5 km^2, 50.503°N, 45.642°E in image9, see Figure 3j
4. 6.24×10^5 km^2, 50.264°N, 45.684°E in image10, see Figure 3k.

The dust storm area grows by a factor of around 3 from image7 to image8, that means in around 1 hr, and remains relatively constant after that. We selected here images7–10 because earlier images have some uncertainty regarding the dust storm boundaries and later images do not show certain parts of the dust storm.

Another EMM instrument, the Emirates Mars Infrared Spectrometer (EMIRS), measured a dust optical depth of 0.55 (at 9.3 μm or 1,075 cm^{-1}) at 49.7°N and 37.5°E. That is part of the EMIRS data file for 18 December 2022 and 16:46:35 UTC. Note that is an average dust optical depth, including also the edge of the observed dust storm. The approximate measurement area is highlighted by a dashed red circle in Figure 3i, which is around 16:43 UTC. The EMIRS instrument has a pixel size of around 100–300 km (Edwards et al., 2021).

The question of whether crater induced circulation plays any role in the initiation and growth of the observed dust storm is not straightforward. Induced circulation by Lyot crater could augment, maintain, or constrain winds, surface dust lifting, and the dust storm. The following demonstrates that this deserves attention. Tyler and Barnes (2015) studied the diurnally varying circulation in and around an idealized crater. A crater-outward directed surge of air develops near the surface during the day. It may extend outward of the crater by up to around 100 km, which is close to the crater diameter of Tyler and Barnes (2015). In our case, a similar surge of air could add to the westerly zonal winds and increase the wind stress, surface dust lifting, and vertical mixing of dust on the leeward side of Lyot crater. The leeward side is to the East of Lyot crater, where the dust storm occurs. As mentioned before, the distance between the observed dust storm and Lyot crater is not more than roughly one crater diameter in Figure 3f and half a crater diameter in Figures 3i–3m. Such questions could be further explored in future work through high-resolution numerical simulations.

5. Summary and Conclusions

The basis of this study is a set of unique high-cadence images from EMM. On 18 December 2022 (MY 36, $L_S = 356°$), the EMM camera EXI took 13 such images in less than eight hours. Most images are separated in time by around half an hour. The images captured variations of clouds and atmospheric dust, over a sub-hour time scale. They are unique snapshots because they show the growth of a local dust storm east of Lyot crater. The dust storm is preceded by lee waves (atmospheric gravity waves).

The lee waves are dominant until mid-morning. Later in the morning, there is a rapid transition between the lee waves and clearly distinct dust storm texture/convective features. The latter become the dominant structure as the

dust storm evolves. That provides insight into the dynamics of the planetary boundary layer. The disappearance of the lee waves and the local dust storm coincide with the development of the CPBL. That is supported by the MCD, which is consistent with radio occultation measurements (Hinson et al., 2019).

Moreover, such case studies with high-cadence images provide valuable knowledge on the dynamics of dust storms. Ogohara and Ro (2023) studied lee waves east of the Phlegra Montes. Interestingly, they pointed out that lee waves may be a probe for deducing atmospheric conditions and related study of dust storm initiation. On a different note, Heavens (2017) studied the texture of selected dust storms in the Amazonis/Arcadia region. Most of their dust storm observations are on a one-per-day-basis. Although, they favored another explanation for dust storm texture formation, they could not exclude the role of gravity waves for one of the dust storms they studied. High-cadence observations like in this article may help to constrain the relevant underlying physical processes.

Data Availability Statement

The basis of this study are EMM images and data on 18 December 2022, available from the EMM Science Data Center (SDC, https://sdc.emiratesmarsmission.ae/). Data product filenames follow a standard convention: emm_<Instrument>_<DataLevel><StartTimeUTC>_<OrbitNumber>_<Mode>_<Description>_<Kernel-Level>_<Version>.<FileType>.

The images and data come in the data format fits (Flexible Image Transport System). We used the python packages "astropy.io.fits" and "imageio" for image/data reading and image visualization. For the map-projection of level2A images from EMM/EXI, we used the Matlab mapping package M_Map (https://www.eoas.ubc.ca/~rich/map.html) (Pawlowicz, 2020).

Figure 1 used the Mars Climate Database (MCD), version 6.1, available from http://www-mars.lmd.jussieu.fr/. Figure 1a used data from Mars Orbiter Laser Altimeter (MOLA) high-resolution topography (32 pixels per degree, also available from the MCD, see the file "mola32.nc").

Acknowledgments
Funding for the development of the EMM mission was provided by the United Arab Emirates Government, and to co-authors outside of the United Arab Emirates by the Mohammed Bin Rashid Space Centre. This work was also supported by a Joint Research Agreement between the Mohammed Bin Rashid Space Centre and the National Space Science and Technology Center in the United Arab Emirates University. CG, BKG, and RMBY were supported by the United Arab Emirates University through research Grant G00003407.

References

Almatroushi, H., AlMazmi, H., AlMheiri, N., AlShamsi, M., AlTunaiji, E., Badri, K., et al. (2021). Emirates Mars mission characterization of Mars atmosphere dynamics and processes. *Space Science Reviews*, *217*(8), 89. https://doi.org/10.1007/s11214-021-00851-6

Amiri, H. E. S., Brain, D., Sharaf, O., Withnell, P., McGrath, M., Alloghani, M., et al. (2022). The Emirates Mars mission. *Space Science Reviews*, *218*(1), 4. https://doi.org/10.1007/s11214-021-00868-x

Appéré, T., Schmitt, B., Langevin, Y., Douté, S., Pommerol, A., Forget, F., et al. (2011). Winter and spring evolution of northern seasonal deposits on Mars from OMEGA on Mars Express. *Journal of Geophysical Research*, *116*(E5), E05001. https://doi.org/10.1029/2010JE003762

Benson, J. L., Kass, D. M., & Kleinböhl, A. (2011). Mars' north polar hood as observed by the Mars Climate Sounder. *Journal of Geophysical Research*, *116*(E3), E03008. https://doi.org/10.1029/2010JE003693

Brooker, L. M., Balme, M. R., Conway, S. J., Hagermann, A., Barrett, A., Collins, G., & Soare, R. (2018). Clastic polygonal networks around Lyot crater, Mars: Possible formation mechanisms from morphometric analysis. *Icarus*, *302*, 386–406. https://doi.org/10.1016/j.icarus.2017.11.022

Dickson, J. L., Fassett, C. I., & Head, J. W. (2009). Amazonian-aged fluvial valley systems in a climatic microenvironment on Mars: Melting of ice deposits on the interior of Lyot Crater. *Geophysical Research Letters*, *36*(8), L08201. https://doi.org/10.1029/2009GL037472

Edwards, C. S., Christensen, P. R., Mehall, G. L., Anwar, S., Tunaiji, E. A., Badri, K., et al. (2021). The Emirates Mars mission (EMM) Emirates Mars InfraRed spectrometer (EMIRS) instrument. *Space Science Reviews*, *217*(7), 77. https://doi.org/10.1007/s11214-021-00848-1

Gebhardt, C., Guha, B. K., Young, R. M. B., & Wolff, M. J. (2022). A frontal dust storm in the northern hemisphere at solar longitude 97—An unusual observation by the Emirates Mars mission. *Geophysical Research Letters*, *49*(20), e2022GL099528. https://doi.org/10.1029/2022GL099528

Haberle, R. M., Clancy, R. T., Forget, F., Smith, M. D., & Zurek, R. W. (Eds.) (2017). *The atmosphere and climate of Mars*. Cambridge University Press. https://doi.org/10.1017/9781139060172

Harrison, T. N., Malin, M. C., Edgett, K. S., Shean, D. E., Kennedy, M. R., Lipkaman, L. J., et al. (2010). Impact-induced overland fluid flow and channelized erosion at Lyot Crater, Mars. *Geophysical Research Letters*, *37*(21), L21201. https://doi.org/10.1029/2010GL045074

Heavens, N. G. (2017). Textured dust storm activity in northeast Amazonis–southwest Arcadia, Mars: Phenomenology and dynamical interpretation. *Journal of the Atmospheric Sciences*, *74*(4), 1011–1037. https://doi.org/10.1175/JAS-D-16-0211.1

Hinson, D. P., Tyler, D., Jr., Lewis, S. R., Pätzold, M., Tellmann, S., Häusler, B., & Tyler, G. L. (2019). The Martian daytime convective boundary layer: Results from radio occultation measurements and a mesoscale model. *Icarus*, *326*, 105–122. https://doi.org/10.1016/j.icarus.2019.02.028

Jeppesen, C., Jones, A., Shuping, R., & Wolff, M. (2021). *EXI data product guide (document No. 169996)*. Mohammed Bin Rashid Space Centre. Retrieved from https://sdc.emiratesmarsmission.ae

Jones, A. R., Wolff, M., Alshamsi, M., Osterloo, M., Bay, P., Brennan, N., et al. (2021). The Emirates exploration imager (EXI) instrument on the Emirates Mars mission (EMM) hope mission. *Space Science Reviews*, *217*(8), 81. https://doi.org/10.1007/s11214-021-00852-5

Kahn, R. (1984). The spatial and seasonal distribution of Martian clouds and some meteorological implications. *Journal of Geophysical Research*, *89*(A8), 6671–6688. https://doi.org/10.1029/JA089iA08p06671

Lemmon, M. T., Smith, M. D., Viudez-Moreiras, D., de la Torre-Juarez, M., Vicente-Retortillo, A., Munguira, A., et al. (2022). Dust, sand, and winds within an active Martian storm in Jezero crater. *Geophysical Research Letters*, *49*(17), e2022GL100126. https://doi.org/10.1029/2022GL100126

Newman, C. E., Lewis, S. R., Read, P. L., & Forget, F. (2002). Modeling the Martian dust cycle, 1, Representations of dust transport processes. *Journal of Geophysical Research*, *107*(E12), 5123. https://doi.org/10.1029/2002JE001910

Ogohara, K., & Ro, M. (2023). Cloud trains associated with Martian mountain lee waves on the eastern side of the Phlegra Montes. *Earth Planets and Space*, *75*(1), 10. https://doi.org/10.1186/s40623-023-01767-x

Ordonez-Etxeberria, I., Hueso, R., Sánchez-Lavega, A., Millour, E., & Forget, F. (2019). Meteorological pressure at Gale crater from a comparison of REMS/MSL data and MCD modelling: Effect of dust storms. *Icarus*, *317*, 591–609. https://doi.org/10.1016/j.icarus.2018.09.003

Ordonez-Etxeberria, I., Hueso, R., Sánchez-Lavega, A., & Vicente-Retortillo, A. (2020). Characterization of a local dust storm on Mars with REMS/MSL measurements and MARCI/MRO images. *Icarus*, *338*, 113521. https://doi.org/10.1016/j.icarus.2019.113521

Pawlowicz, R. (2020). "M_Map: A mapping package for MATLAB", version 1.4m [Computer software]. Stl. Retrieved from https://www.eoas.ubc.ca/~rich/map.html

Pickersgill, A. O., & Hunt, G. E. (1979). The formation of Martian lee waves generated by a crater. *Journal of Geophysical Research*, *84*(B14), 8317–8331. https://doi.org/10.1029/JB084iB14p08317

Pickersgill, A. O., & Hunt, G. E. (1982). A comparison of observed LEE-waves on earth and Mars. *Weather*, *37*(4), 98–108. https://doi.org/10.1002/j.1477-8696.1982.tb03571.x

Sánchez-Lavega, A., Erkoreka, A., Hernández-Bernal, J., del Río-Gaztelurrutia, T., García-Morales, J., Ordoñez-Etxeberría, I., et al. (2022). Cellular patterns and dry convection in textured dust storms at the edge of Mars North Polar Cap. *Icarus*, *387*, 115183. https://doi.org/10.1016/j.icarus.2022.115183

Tyler, D., & Barnes, J. R. (2015). Convergent crater circulations on Mars: Influence on the surface pressure cycle and the depth of the convective boundary layer. *Geophysical Research Letters*, *42*(18), 7343–7350. https://doi.org/10.1002/2015gl064957

Wang, H., & Ingersoll, A. P. (2002). Martian clouds observed by Mars global surveyor Mars orbiter camera. *Journal of Geophysical Research*, *107*(E10), 5078. https://doi.org/10.1029/2001JE001815

Weiss, D. K., Head, J. W., Palumbo, A. M., & Cassanelli, J. P. (2017). Extensive Amazonian-aged fluvial channels on Mars: Evaluating the role of Lyot crater in their formation. *Geophysical Research Letters*, *44*(11), 5336–5344. https://doi.org/10.1002/2017GL073821

Wood, S. E., Catling, D. C., Rafkin, S. C. R., Ginder, E. A., & Peacock, C. G. (2003). MGS observations and modeling of Martian lee wave clouds, sixth international conference on Mars. Retrieved from https://www.lpi.usra.edu/meetings/sixthmars2003/pdf/3283.pdf